

Supplementary material

Contents

<i>Supplementary methods</i>	2
Rationale of the Majewski criteria for FAS	2
MRI data preprocessing	3
<i>Supplementary tables</i>	6
Supplementary Table 1 – Group comparison of head motion estimates	6
<i>Supplementary figures</i>	7
Supplementary Figure 1 – Goodness-of-fit statistics for different k-means clustering solutions (2 to 10 clusters) for putative functional connectivity states in the time-resolved analysis.	7
Supplementary Figure 2 – Connectivity matrices representing the two putative functional connectivity (FC) states in the optimal clustering solution of the time-resolved analysis across the entire sample.	8

Supplementary methods

Rationale of the Majewski criteria for FAS

The Majewski diagnostic criteria for FAS [37] were widely used in German speaking countries at the time of diagnosis [38] of the participants with FAS in this study. In summary, they are based on the following clinical features [37]:

- intrauterine and/or postnatal growth retardation
- microcephalus
- typical facial anomalies
- statomotoric and mental retardation
- hyperactivity
- cleft palate
- cardiac anomalies
- musculoskeletal anomalies
- genital anomalies
- other developmental anomalies

MRI data preprocessing

The following fMRIPrep “boilerplate” (indented text) describes the preprocessing steps in detail. The text has intentionally been left completely unchanged according to the fMRIPrep recommendations for optimal reproducibility. Please note that fMRIPrep generated multiple preprocessing outputs which could be used in different denoising and analysis strategies. Not all of these parallel outputs have been used for further processing in this study. Details about which outputs were used for actual denoising and further functional connectivity modelling are presented in the main text.

Results included in this manuscript come from preprocessing performed using *fMRIPrep* 20.0.7 (Esteban, Markiewicz, et al. (2018); Esteban, Blair, et al. (2018); RRID:SCR_016216), which is based on *Nipype* 1.4.2 (Gorgolewski et al. (2011); Gorgolewski et al. (2018); RRID:SCR_002502).

Anatomical data preprocessing

The T1-weighted (T1w) image was corrected for intensity non-uniformity (INU) with `N4BiasFieldCorrection` (Tustison et al. 2010), distributed with ANTs 2.2.0 (Avants et al. 2008, RRID:SCR_004757), and used as T1w-reference throughout the workflow. The T1w-reference was then skull-stripped with a *Nipype* implementation of the `antsBrainExtraction.sh` workflow (from ANTs), using OASIS30ANTs as target template. Brain tissue segmentation of cerebrospinal fluid (CSF), white-matter (WM) and gray-matter (GM) was performed on the brain-extracted T1w using `fast` (FSL 5.0.9, RRID:SCR_002823, Zhang, Brady, and Smith 2001). Brain surfaces were reconstructed using `recon-all` (FreeSurfer 6.0.1, RRID:SCR_001847, Dale, Fischl, and Sereno 1999), and the brain mask estimated previously was refined with a custom variation of the method to reconcile ANTs-derived and FreeSurfer-derived segmentations of the cortical gray-matter of Mindboggle (RRID:SCR_002438, Klein et al. 2017). Volume-based spatial normalization to one standard space (MNI152NLin2009cAsym) was performed through nonlinear registration with `antsRegistration` (ANTs 2.2.0), using brain-extracted versions of both T1w reference and the T1w template. The following template was selected for spatial normalization: *ICBM 152 Nonlinear Asymmetrical template version 2009c* [Fonov et al. (2009), RRID:SCR_008796; TemplateFlow ID: MNI152NLin2009cAsym],

Functional data preprocessing

For each of the 1 BOLD runs found per subject (across all tasks and sessions), the following preprocessing was performed. First, a reference volume and its skull-stripped version were generated using a custom methodology of *fMRIPrep*. Susceptibility distortion correction (SDC) was omitted. The BOLD reference was then co-registered to the T1w reference using `bbregister` (FreeSurfer) which implements boundary-based registration (Greve and Fischl 2009). Co-registration was configured with six degrees of freedom. Head-motion parameters with respect to the BOLD reference (transformation matrices, and six corresponding rotation and translation parameters) are estimated before any spatiotemporal filtering using `mcflirt` (FSL 5.0.9, Jenkinson et al. 2002). The BOLD time-series (including slice-timing correction when applied) were resampled onto their original, native space by applying the transforms to correct for head-motion. These resampled BOLD time-series will be referred to as *preprocessed BOLD in original space*, or just *preprocessed BOLD*. The BOLD time-series were resampled into standard space, generating a *preprocessed BOLD run in MNI152NLin2009cAsym space*. First, a reference volume and its skull-stripped version were generated using a custom methodology of *fMRIPrep*. Several confounding time-series were calculated based on the *preprocessed BOLD*: framewise displacement (FD), DVARS and three region-wise global signals. FD and DVARS are calculated for each functional run, both using their implementations in *Nipype* (following the definitions by Power et al. 2014). The three global signals are extracted within the CSF, the WM, and the whole-brain masks. Additionally, a set of physiological regressors were extracted to allow for component-based noise correction (*CompCor*, Behzadi et al. 2007). Principal components are estimated after high-pass filtering the *preprocessed BOLD* time-series (using a discrete cosine filter with 128s cut-off) for the two *CompCor* variants: temporal (tCompCor) and anatomical (aCompCor). tCompCor components are then calculated from the top 5% variable voxels within a mask covering the subcortical regions. This subcortical mask is obtained by heavily eroding the brain mask, which ensures it does not include cortical GM regions. For aCompCor, components are calculated within the intersection of the

aforementioned mask and the union of CSF and WM masks calculated in T1w space, after their projection to the native space of each functional run (using the inverse BOLD-to-T1w transformation). Components are also calculated separately within the WM and CSF masks. For each CompCor decomposition, the k components with the largest singular values are retained, such that the retained components' time series are sufficient to explain 50 percent of variance across the nuisance mask (CSF, WM, combined, or temporal). The remaining components are dropped from consideration. The head-motion estimates calculated in the correction step were also placed within the corresponding confounds file. The confound time series derived from head motion estimates and global signals were expanded with the inclusion of temporal derivatives and quadratic terms for each (Satterthwaite et al. 2013). Frames that exceeded a threshold of 0.5 mm FD or 1.5 standardised DVARS were annotated as motion outliers. All resamplings can be performed with *a single interpolation step* by composing all the pertinent transformations (i.e. head-motion transform matrices, susceptibility distortion correction when available, and co-registrations to anatomical and output spaces). Gridded (volumetric) resamplings were performed using `antsApplyTransforms` (ANTs), configured with Lanczos interpolation to minimize the smoothing effects of other kernels (Lanczos 1964). Non-gridded (surface) resamplings were performed using `mri_vol2surf` (FreeSurfer).

Many internal operations of *fMRIPrep* use *Nilearn* 0.6.2 (Abraham et al. 2014, RRID:SCR_001362), mostly within the functional processing workflow. For more details of the pipeline, see [the section corresponding to workflows in fMRIPrep's documentation](#).

Copyright Waiver

The above boilerplate text was automatically generated by *fMRIPrep* with the express intention that users should copy and paste this text into their manuscripts *unchanged*. It is released under the [CC0](#) license.

References

- Abraham, Alexandre, Fabian Pedregosa, Michael Eickenberg, Philippe Gervais, Andreas Mueller, Jean Kossaifi, Alexandre Gramfort, Bertrand Thirion, and Gael Varoquaux. 2014. "Machine Learning for Neuroimaging with Scikit-Learn." *Frontiers in Neuroinformatics* 8. <https://doi.org/10.3389/fninf.2014.00014>.
- Avants, B.B., C.L. Epstein, M. Grossman, and J.C. Gee. 2008. "Symmetric Diffeomorphic Image Registration with Cross-Correlation: Evaluating Automated Labeling of Elderly and Neurodegenerative Brain." *Medical Image Analysis* 12 (1): 26–41. <https://doi.org/10.1016/j.media.2007.06.004>.
- Behzadi, Yashar, Khaled Restom, Joy Liau, and Thomas T. Liu. 2007. "A Component Based Noise Correction Method (CompCor) for BOLD and Perfusion Based fMRI." *NeuroImage* 37 (1): 90–101. <https://doi.org/10.1016/j.neuroimage.2007.04.042>.
- Dale, Anders M., Bruce Fischl, and Martin I. Sereno. 1999. "Cortical Surface-Based Analysis: I. Segmentation and Surface Reconstruction." *NeuroImage* 9 (2): 179–94. <https://doi.org/10.1006/nimg.1998.0395>.
- Esteban, Oscar, Ross Blair, Christopher J. Markiewicz, Shoshana L. Berleant, Craig Moodie, Feilong Ma, Ayse Ilkay Isik, et al. 2018. "fMRIPrep." *Software*. Zenodo. <https://doi.org/10.5281/zenodo.852659>.
- Esteban, Oscar, Christopher Markiewicz, Ross W Blair, Craig Moodie, Ayse Ilkay Isik, Asier Erramuzpe Aliaga, James Kent, et al. 2018. "fMRIPrep: A Robust Preprocessing Pipeline for Functional MRI." *Nature Methods*. <https://doi.org/10.1038/s41592-018-0235-4>.
- Fonov, VS, AC Evans, RC McKinsty, CR Almli, and DL Collins. 2009. "Unbiased Nonlinear Average Age-Appropriate Brain Templates from Birth to Adulthood." *NeuroImage* 47, Supplement 1: S102. [https://doi.org/10.1016/S1053-8119\(09\)70884-5](https://doi.org/10.1016/S1053-8119(09)70884-5).

- Gorgolewski, K., C. D. Burns, C. Madison, D. Clark, Y. O. Halchenko, M. L. Waskom, and S. Ghosh. 2011. "Nipype: A Flexible, Lightweight and Extensible Neuroimaging Data Processing Framework in Python." *Frontiers in Neuroinformatics* 5: 13. <https://doi.org/10.3389/fninf.2011.00013>.
- Gorgolewski, Krzysztof J., Oscar Esteban, Christopher J. Markiewicz, Erik Ziegler, David Gage Ellis, Michael Philipp Notter, Dorota Jarecka, et al. 2018. "Nipype." *Software*. Zenodo. <https://doi.org/10.5281/zenodo.596855>.
- Greve, Douglas N, and Bruce Fischl. 2009. "Accurate and Robust Brain Image Alignment Using Boundary-Based Registration." *NeuroImage* 48 (1): 63–72. <https://doi.org/10.1016/j.neuroimage.2009.06.060>.
- Jenkinson, Mark, Peter Bannister, Michael Brady, and Stephen Smith. 2002. "Improved Optimization for the Robust and Accurate Linear Registration and Motion Correction of Brain Images." *NeuroImage* 17 (2): 825–41. <https://doi.org/10.1006/nimg.2002.1132>.
- Klein, Arno, Satrajit S. Ghosh, Forrest S. Bao, Joachim Giard, Yrjö Häme, Eliezer Stavsky, Noah Lee, et al. 2017. "Mindboggling Morphometry of Human Brains." *PLOS Computational Biology* 13 (2): e1005350. <https://doi.org/10.1371/journal.pcbi.1005350>.
- Lanczos, C. 1964. "Evaluation of Noisy Data." *Journal of the Society for Industrial and Applied Mathematics Series B Numerical Analysis* 1 (1): 76–85. <https://doi.org/10.1137/0701007>.
- Power, Jonathan D., Anish Mitra, Timothy O. Laumann, Abraham Z. Snyder, Bradley L. Schlaggar, and Steven E. Petersen. 2014. "Methods to Detect, Characterize, and Remove Motion Artifact in Resting State fMRI." *NeuroImage* 84 (Supplement C): 320–41. <https://doi.org/10.1016/j.neuroimage.2013.08.048>.
- Satterthwaite, Theodore D., Mark A. Elliott, Raphael T. Gerraty, Kosha Ruparel, James Loughhead, Monica E. Calkins, Simon B. Eickhoff, et al. 2013. "An improved framework for confound regression and filtering for control of motion artifact in the preprocessing of resting-state functional connectivity data." *NeuroImage* 64 (1): 240–56. <https://doi.org/10.1016/j.neuroimage.2012.08.052>.
- Tustison, N. J., B. B. Avants, P. A. Cook, Y. Zheng, A. Egan, P. A. Yushkevich, and J. C. Gee. 2010. "N4ITK: Improved N3 Bias Correction." *IEEE Transactions on Medical Imaging* 29 (6): 1310–20. <https://doi.org/10.1109/TMI.2010.2046908>.
- Zhang, Y., M. Brady, and S. Smith. 2001. "Segmentation of Brain MR Images Through a Hidden Markov Random Field Model and the Expectation-Maximization Algorithm." *IEEE Transactions on Medical Imaging* 20 (1): 45–57. <https://doi.org/10.1109/42.906424>.

Supplementary tables

Supplementary Table 1 – Group comparison of head motion estimates

Data derived from preprocessing (final sample after exclusion of participants with excessive head motion).

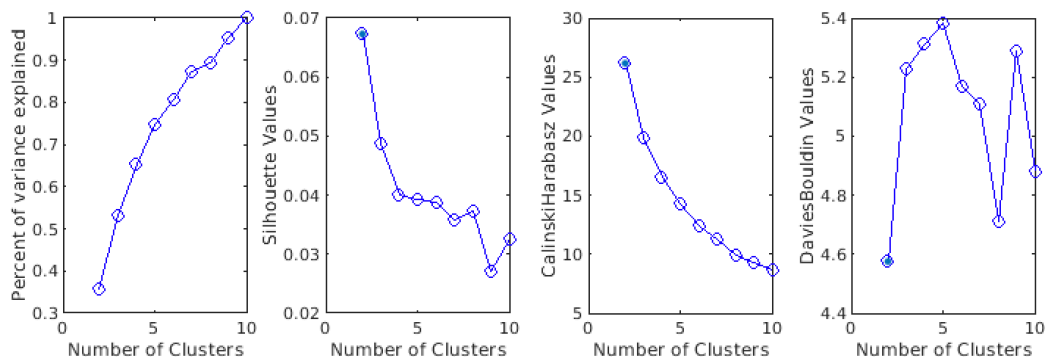
	FAS ^a	CON ^a	p ^b
Mean FD (mm)	0.148 (0.07 – 0.27)	0.126 (0.08 – 0.29)	0.081
Maximum FD (mm)	0.950 (0.22 – 3.25)	0.649 (0.18 – 1.83)	0.061
Percentage of motion spikes	1.709 (0.00 – 10.26)	0.855 (0.00 – 16.67)	0.147

^a median (range) ^b Mann-Whitney-U-test result. FAS: fetal alcohol syndrome, CON: controls, FD: framewise displacement

Supplementary figures

Supplementary Figure 1 – Goodness-of-fit statistics for different k-means clustering solutions (2 to 10 clusters) for putative functional connectivity states in the time-resolved analysis.

From left to right: percent of variance explained (relative to a 10-cluster solution), silhouette values (possible range: -1 to 1) with higher values representing good cluster separability, higher Calinski-Harabasz values representing higher cluster density and separability, and Davies–Bouldin criterion (lower values representing higher clustering quality).



Supplementary Figure 2 – Connectivity matrices representing the two putative functional connectivity (FC) states in the optimal clustering solution of the time-resolved analysis across the entire sample.

Original model estimates from the DynamicBC toolbox calculated in the entire sample. Matrices ordered according to the ROI order key provided in the Supplementary data. Left: Cluster 1 shows widely distributed FC dominated by the default mode network (DMN); Right: Cluster 2 exhibits stronger dichotomization between the DMN and the other cognition-related networks. LH: left hemisphere, RH: right hemisphere

